Journal of Materials Chemistry B

ROYAL SOCIETY OF CHEMISTRY

PAPER

View Article Online
View Journal | View Issue



Cite this: J. Mater. Chem. B, 2023, 11, 1302

# Covalent immobilization of lipase on an ionic liquid-functionalized magnetic Cu-based metal–organic framework with boosted catalytic performance in flavor ester synthesis†

Hongbo Suo,[a] Huining Geng,[a] Lu Zhang,[a] Guoyun liu,[a] Hui Yan,[a] Rui Cao,[a] Jiahao Zhu,[a] Yi Hu *[b] and Lili Xu *[a]

Received 18th October 2022,
Accepted 31st December 2022

DOI: 10.1039/d2tb02246j

rsc.li/materials-b



Enzymatic esterification plays an important role in the fields of chemistry and biotechnology. In this study, lipase was immobilized on an ionic liquid (IL)-modified magnetic metal–organic framework (MOF) and used to synthesize isoamyl acetate. The immobilized lipase (PPL-ILs/$Fe_3O_4$@MOF) showed 2.1-fold and 1.8-fold higher activity compared to the free and immobilized lipase without ILs (PPL-$Fe_3O_4$@MOF), respectively. In addition, the anti-denaturant ability and reusability of the PPL-ILs/$Fe_3O_4$@MOF were also higher than those of other samples. The ester yield reached 75.1% when the biocatalyst was used to synthesize isoamyl acetate in hexane. The synthesized supports supplied a good microenvironment for the immobilized lipase through multiple interactions. Results of the structural analysis showed that the conformation state of lipase molecules changed after immobilization. The magnetism of the prepared biocatalyst makes it easy to recycle so that PPL-ILs/$Fe_3O_4$@MOF maintained 70.2% of the initial activity after eight cycles. The prepared composite materials exhibited good potential in lipase immobilization with enhanced catalytic ability and stability.

## 1. Introduction

Isoamyl acetate is a flavor ester characterized by banana and pear fragrances. It is widely used in food and flavoring industries, especially in the production of fruit jam, honey, butterscotch, and beverages. Given that the traditional method of extracting isoamyl acetate from natural resources cannot match the high global demand, the method of adopting chemical catalysts was developed. However, with the continuous popularization of the concept of green chemistry and cleaner production, improving the esterification reaction route to promote the environmental friendliness of the synthesis of isoamyl acetate has become an important direction in current scientific research.[1,2]

Lipase can catalyze esterification and transesterification reactions, and its application in the synthesis of flavor and fragrance esters is among its important applications.[3,4] Enzymatic reactions are promising with high efficiency, specificity and mildness. Studies have shown that short chain esters synthesized by immobilized lipase has good application prospects. Polydopamine and cobalt-functionalized multiwalled carbon nanotubes,[5] epoxy-activated cloisite,[6] and poly-coated magnetic nanoparticles[7] were used to immobilize lipase for the synthesis of short-chain flavor esters. There is a hydrophobic lid-covered lipase active center, which has the characteristics of interface activation.[8] Existing research reports have mainly adopted the protein engineering technology to mutate different amino acids in the lid domain of lipase, study the change of lipase properties, or construct a lidless lipase.[9,10] By designing appropriate nanomaterials for lipase immobilization, the interaction between materials and lipase can affect the lid domain of lipase, thereby improving the activity, stability, and reusability of lipase.[11–13]

A reasonable design of the immobilization support and immobilization method can effectively improve the catalytic performance of the enzyme.[14] The enzyme is easily affected by environmental factors, such as temperature, pH fluctuation, organic solvents, and small molecule inhibitors. When stimulated by these external factors, the conformation of the enzyme will be disturbed to varying degrees or the structure of the active site of the enzyme will be directly destroyed, resulting in reduced or total loss of catalytic activity. Metal–organic frameworks (MOFs) are extensible network frameworks connected by

[a] School of Pharmaceutical Sciences, Liaocheng University, Liaocheng, Shandong, 252059, China. E-mail: lilixu66@163.com
[b] State Key Laboratory of Materials-Oriented Chemical Engineering, School of Pharmaceutical Sciences, Nanjing Tech University, Nanjing 210009, China. E-mail: huyi@njtech.edu.cn

† Electronic supplementary information (ESI) available. See DOI: https://doi.org/10.1039/d2tb02246j

organic ligands and metal nodes (metal ions or metal clusters). Different nodes and linkers can be assembled to form MOFs with various structures. In addition, the rich functional groups of the framework give them flexible modification characteristics. MOFs have the advantages of ultra-high porosity, adjustable pore size, excellent chemical and thermal stability, and are excellent enzyme immobilization carriers.[15–17] The surface of the enzyme has a variety of amino acid residues with rich charge characteristics, which enables interaction with the surface or internal pore chemical components of MOFs, including H-bonding, electrostatic force, van der Waals force, π–π interaction, and covalent interaction. Therefore, it is easy to form a stable enzyme with the complex structure of the MOFs. Furthermore, the ultra-high porosity of MOFs can greatly improve the loading efficiency of the enzyme, and the adjustable pore characteristics are conducive to cutting out the fixed space matching the size of the enzyme. Also, the excellent chemical and thermal stability gives enzymes with the higher stability of MOF composites.[18]

Furthermore, because of the nanometer size of supports, it's difficult to recover the enzyme–support conjugates from the reaction medium. Researchers have developed many magnetic nanocomposites, such as hydroxyapatite-encapsulated γ-$Fe_2O_3$,[19] $Fe_3O_4$–MCM-41,[20] magnetic MOFs,[21] $Fe_3O_4$/nanotube composites,[22] magnetic graphene oxide[23] and others[24] to enhance the recovery of immobilized enzyme. The well-designed MOF–$Fe_3O_4$ composites combined the unique properties of MOFs and magnetism of $Fe_3O_4$ into one support. The magnetic separation can greatly improve the reusability of the enzyme.

Improving the microenvironment of immobilized enzyme could be achieved by introducing functional compounds into supports which can enhance the specific action between enzyme and supports. By introducing cross-linking molecules or modifiers between enzyme and supports, the interactions (electrostatic, chemical bond, hydrogen bond, and hydrophilic/hydrophobic interaction) can be improved, such that the active conformation and flexible structure of the enzyme can be effectively protected.[25] Ionic liquids (ILs), as green solvents composed of anions and anions, are used in the enzymatic synthesis of chiral alcohols, chiral amines, and sugars and their derivatives, which greatly improve the catalytic effect.[26,27] Applying ILs to an immobilized enzyme can also improve the catalytic performance of the enzyme. For instance, we previously used imidazole IL as a crosslinking molecule to prepare a chitosan/SBA-15 composite for the immobilization of porcine pancreatic lipase (SBA-CIL-CS-PPL). We found that the activity of immobilized lipase was 8.3 times that of the free PPL and that 82% activity was retained after repeated use of 10 times.[28] Xie and co-workers covalently grafted imidazole-based ILs to magnetic silica composites for lipase immobilization. The immobilized lipase showed good activity when it was used to synthesized *trans*-free plastic fats. In addition, the prepared biocatalyst didn't show significant reduction of activity as it was reused several times.[29]

In this study, IL-modified magnetic MOFs were prepared and used to immobilize lipase for the synthesis of flavor esters. The synthesis process of the composite and the immobilization of lipase are shown in Scheme 1. The type and strength of the force between lipases and supports affect the structure and catalytic performance of the immobilized lipase. Therefore, the novelty of this work focuses on revealing the adaptability between the lipase and supports by studying the surface properties of supports. The conformation of lipase before and after

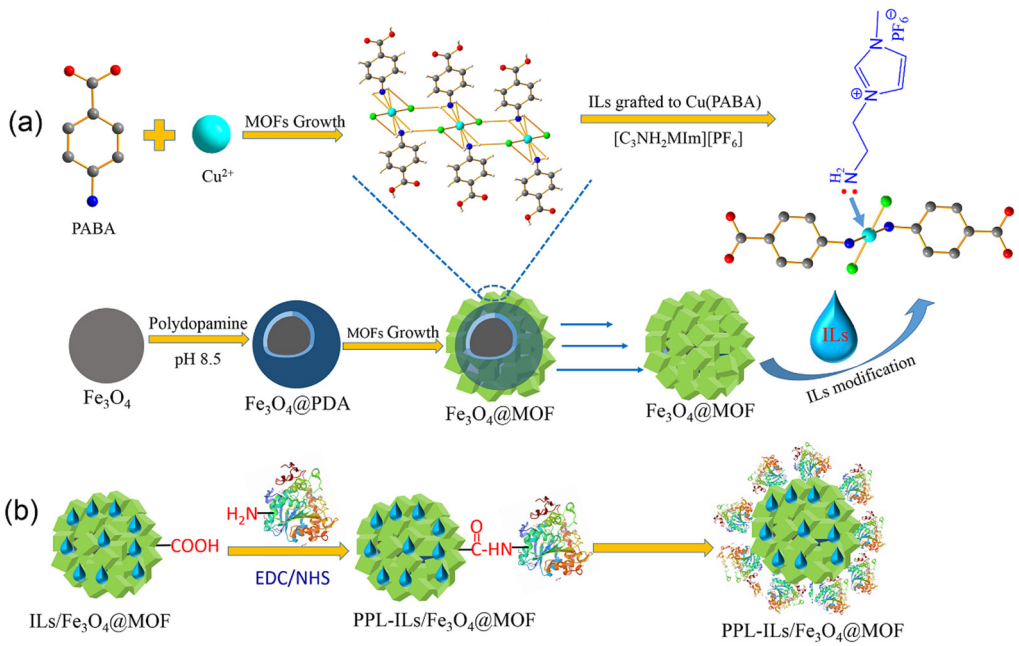


Scheme 1 (a) The synthesis route of ionic liquid modified $Fe_3O_4$@MOF and (b) schematic illustration of lipase covalent immobilization on ILs/$Fe_3O_4$@MOF.

immobilization was investigated using circular dichroism to analyze the mechanism of enhanced catalytic performance. In addition, the composite combines the porosity of MOFs and the magnetism of $Fe_3O_4$, which has a high enzyme loading capacity and convenient separation performance. Furthermore, this new biocatalyst has a potential application in the synthesis of other esters. This study prepared a MOF based composite which has good compatibility with biological macromolecules and expanded the method of improving the microenvironment of immobilized enzymes.

## 2. Experimental section

### 2.1. Reagents

Dopamine hydrochloride (DA), 1-ethyl-3-(3-dimethylamino propyl) carbodiimide hydrochloride (EDC), Coomassie brilliant blue G-250, *N*-hydroxysuccinimide (NHS), and urea were procured from Shanghai Aladdin Biochem Technology Co., Ltd. Cupric chloride dihydrate, *p*-aminobenzoic acid (PABA), *n*-hexane and triacetin were procured from Sinopharm Chemical Reagent Co., Ltd (Shanghai, China). Porcine pancreatic lipase (PPL) was procured from Sigma-Aldrich. Sodium hyaluronate was purchased from AVT (Shanghai) Pharmaceutical Tech Co., Ltd. 1-Aminopropylimidazolium bis(trifluoromethylsulfonyl)imine (IL: $[C_3NH_2MIm][NTf_2]$) was procured from Lanzhou Greenchem ILs.

### 2.2. Synthesis of the magnetic Cu-based MOF

In brief, the pH of a 200 mL of phosphate buffered solution (PBS) was adjusted to 8.5 and then 1.2 g of $Fe_3O_4$ and 0.4 g of DA were added under stirring. After reacting for 12 h at room temperature, the black solid ($Fe_3O_4$@PDA) was separated from the solution and washed with fresh PBS and deionized water. Subsequently, 0.5 g of $Fe_3O_4$@PDA was added to a 100 mL PBS solution (25 mM, pH 6.5) containing 1.03 g of PABA and then 50 mL of PBS solution containing 2.7 g of $CuCl_2{\cdot}2H_2O$ was added. The mixture was allowed to react for 2 h at 60 °C under stirring. Finally, the obtained solid was separated magnetically and named $Fe_3O_4$@MOF.

### 2.3. Preparation of an IL-functionalized magnetic Cu-based MOF

The IL-functionalized magnetic Cu-based MOF was prepared through a physical doping method, as reported with minor modification. Firstly, 0.15 g of IL was dissolved in 60 mL ethanol, and then 0.5 of $Fe_3O_4$@MOF was added. In order to ensure uniform mixing and sufficient contact of IL and $Fe_3O_4$@MOF, the solution was stirred at room temperature for 2 h. Next, the solution was transferred to a rotary evaporate to eliminate the ethanol at 45 °C. The obtained solids were collected, washed thrice with ethanol, and named IL/$Fe_3O_4$@MOF.

### 2.4. Characterization of supports

The prepared composites were characterized using Fourier transform infrared (FT-IR) spectroscopy, X-ray diffraction (XRD) spectroscopy, scanning electron microscopy (SEM), transmission electron microscopy (TEM), vibrating sample magnetometry (VSM) and thermogravimetric analysis (TGA). The secondary structure of lipase was conducted using circular dichroism (CD) spectroscopy. Details of the devices used are shown in ESI.† Vienna *ab initio* simulation package (VASP) was used to calculate the interaction between MOFs and ILs using density functional theory (DFT).

### 2.5. Lipase immobilization

In order to achieve covalent immobilization of enzymes, using an active carboxyl group of IL/$Fe_3O_4$@MOF to interact with amino of lipase. Briefly, EDC (0.096 g), NHS (0.058 g) and IL/$Fe_3O_4$@MOF (0.5 g) were successively added to 50 mL of PBS (pH 6.5). After IL/$Fe_3O_4$@MOF was activated for 1 h under room temperature, it was magnetically separated and washed with PBS. Then, the activated IL/$Fe_3O_4$@MOF was added to a 50 mL lipase solution (2.53 mg $mL^{-1}$) and continued to react for 4 h under vibration. Finally, the immobilized lipase was separated using a magnet and freeze-dried. The lipase loading was calculated using the Bradford method.

### 2.6. Activity assessment of immobilized lipase

The activity of the prepared biocatalyst was conducted using measure the hydrolysis of triacetin. The ester hydrolyzed and produced acid under the catalysis of lipase in aqueous solution. The released acid could be measured through titration by NaOH solution (0.05 M). The activity could be calculated according to the consumed alkali solution. Each experiment was conducted at least three times.

### 2.7. Effect of pH and temperature on the activity of lipase

In order to estimate the pH value effect on lipase activity, the pH of substrate solution was set in the range of 6.0–8.5 under a constant temperature. When the effect of temperature was investigated, the pH was maintained at the optimum value of samples when the reaction temperature ranged from 30 to 60 °C. At least three times shall be conducted for each test.

### 2.8. Test of anti-denaturant ability and reusability

The biocatalyst sample was incubated in urea solution for 1 h at the concentration of 1–6 M under optimal pH and temperature. Then, the biocatalyst was used to catalyze ester hydrolysis and its residual activity was measured. The reusability of the prepared biocatalyst was evaluated through successive use for eight cycles under optimized conditions. Each time, the biocatalyst was washed with PBS and then used for the next cycle.

### 2.9. Application for the synthesis of isoamyl acetate

The reaction conditions (reaction time, temperature, solvents and substrate ratio) for lipase-catalyzed esterification of acetic acid and isoamyl alcohol were optimized. The yield of the ester was calculated according to the conversion of acetic acid. The amount of acetic acid was determined by the volume of consumed NaOH solution (0.02 M).

 

# 3. Results and discussion

### 3.1. Synthesis and characterization of the composite material (IL/$Fe_3O_4$@MOF)

The FTIR spectra of (a) $Fe_3O_4$, (b) $Fe_3O_4$@PDA, (c) $Fe_3O_4$@MOF, and (d) ILs/$Fe_3O_4$@MOF are shown in Fig. 1. In the $Fe_3O_4$ curve, an adsorption band at 582 $cm^{-1}$ was attributed to the characteristic peak of Fe–O. After coating with PDA, the $Fe_3O_4$@PDA curve appeared at 1050 $cm^{-1}$, which was attributed to the C–O stretching vibration (Fig. 1b).[30] As shown in the $Fe_3O_4$@MOF curve, the adsorption signals at 1605 $cm^{-1}$ and 1388 $cm^{-1}$ were assigned to the antisymmetric and symmetric stretching vibrations of the carboxyl group located in PABA.[31] The adsorption bands at 1505–1570 $cm^{-1}$ were due to the stretching vibration of unsaturated olefinic bonds located in benzene and the skeleton vibration of the benzene ring framework. Another peak at 779 $cm^{-1}$ was due to the *para*-substituted benzene ring.[31,32] Compared to $Fe_3O_4$@MOF, after IL modification, the ILs/$Fe_3O_4$@MOF curve showed two new peaks. The adsorption peaks at 1194 $cm^{-1}$ and 1125 $cm^{-1}$ were attributed to the C–F stretching vibration which was located in the anion $[Tf_2N]^-$ of the ILs and the C–N stretching vibration which was located in imidazole ring.[33] The adsorption band at 1624 $cm^{-1}$ (N–H bending vibration) in the ILs/$Fe_3O_4$@MOF curve was enhanced compared to that in $Fe_3O_4$@MOF, indicating that the ILs with $-NH_2$ were introduced. The results proved that ILs were successfully grafted to $Fe_3O_4$@MOF. Moreover, the elemental analysis of ILs/$Fe_3O_4$@MOF was conducted and the EDS spectrum with atomic ratio of ILs/$Fe_3O_4$@MOF is shown in Fig. 2d. Elements corresponding to the formation of composite materials were all detected. The result of EDS confirmed the formation of Cu based MOFs and the presence of anions ($[TNf_2]^-$). Furthermore, the adsorption energy of cation $[AMI]^+$ and anion $[TNf_2]^-$ with $Fe_3O_4$@MOF was calculated using the VASP based on DFT. The adsorption energy of $[AMI]^+$/$Fe_3O_4$@MOF was −3.89 eV, lower than that of $[TNf_2]^-$/$Fe_3O_4$@MOF (−2.14 eV). The calculated result indicated that the interaction between $[AMI]^+$ and $Fe_3O_4$@MOF was stronger which could be proved by the charge density difference map (Fig. S1, ESI†).

XRD was conducted to further confirm the formation of Cu-based MOF coated on $Fe_3O_4$ nanoparticles and the patterns of supports are shown in Fig. 2a. The characteristic peaks of $Fe_3O_4$ for corresponding plane indexes was consistent with the reports.[34] For $Fe_3O_4$@MOF and ILs/$Fe_3O_4$@MOF, the XRD patterns exhibited $Fe_3O_4$ characteristic peaks and showed additional peaks, which was consistent with the characteristic peaks of Cu-PABA.[32] The results indicate that the successful formation of Cu-based MOF coated on $Fe_3O_4$ and the IL grafting did not change the crystal structure of the magnetic MOF nanoparticles.

TGA was conducted under a $N_2$ flow to analyze the thermal properties of supports. The TGA curves are shown in Fig. 2b. As expressed, $Fe_3O_4$ showed 3.21% weight loss under 100 °C, which was due to the removal of water. From 100 to 800 °C, $Fe_3O_4$ exhibited no weight loss and showed great thermal stability. In the case of $Fe_3O_4$@MOF, a weight loss step was seen from 100 to 305 °C due to solvent evaporation from the MOF layer. When temperature ranged from 305 to 445 °C, $Fe_3O_4$@MOF showed a 9.26% weight loss which was ascribed to the MOF framework collapse. Compared with $Fe_3O_4$@MOF, the weight loss of ILs/$Fe_3O_4$@MOF was more severe due to the superposition of the decomposition of ILs and the collapse of the MOF framework. TGA results further proved the successful synthesis of ILs/$Fe_3O_4$@MOF.

Magnetic separation can be used to separate the magnetic biocatalyst from the reaction system. The magnetic properties

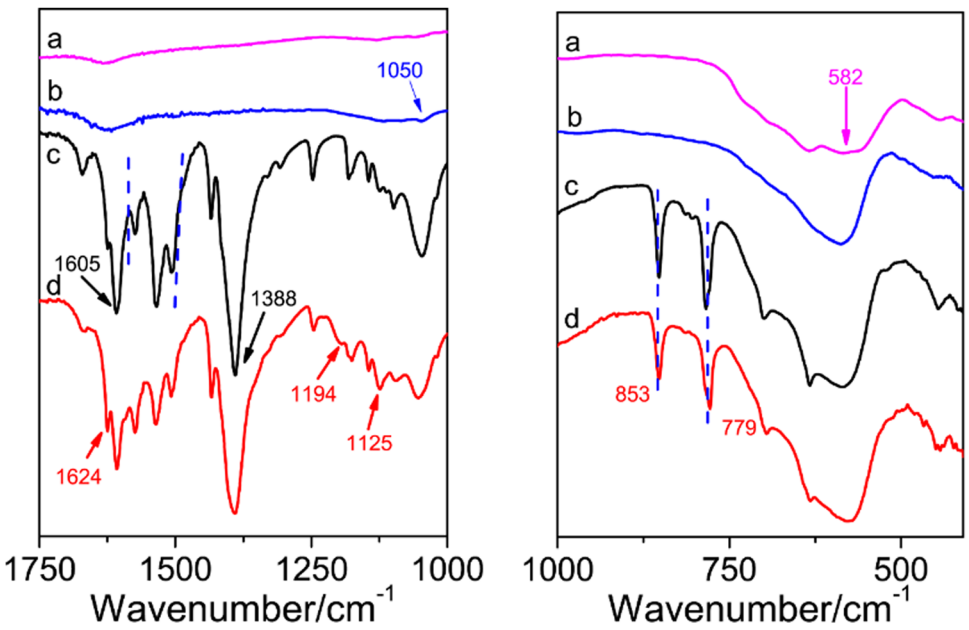


Fig. 1 FTIR spectra of (a) $Fe_3O_4$, (b) $Fe_3O_4$@PDA, (c) $Fe_3O_4$@MOF, and (d) ILs/$Fe_3O_4$@MOF.

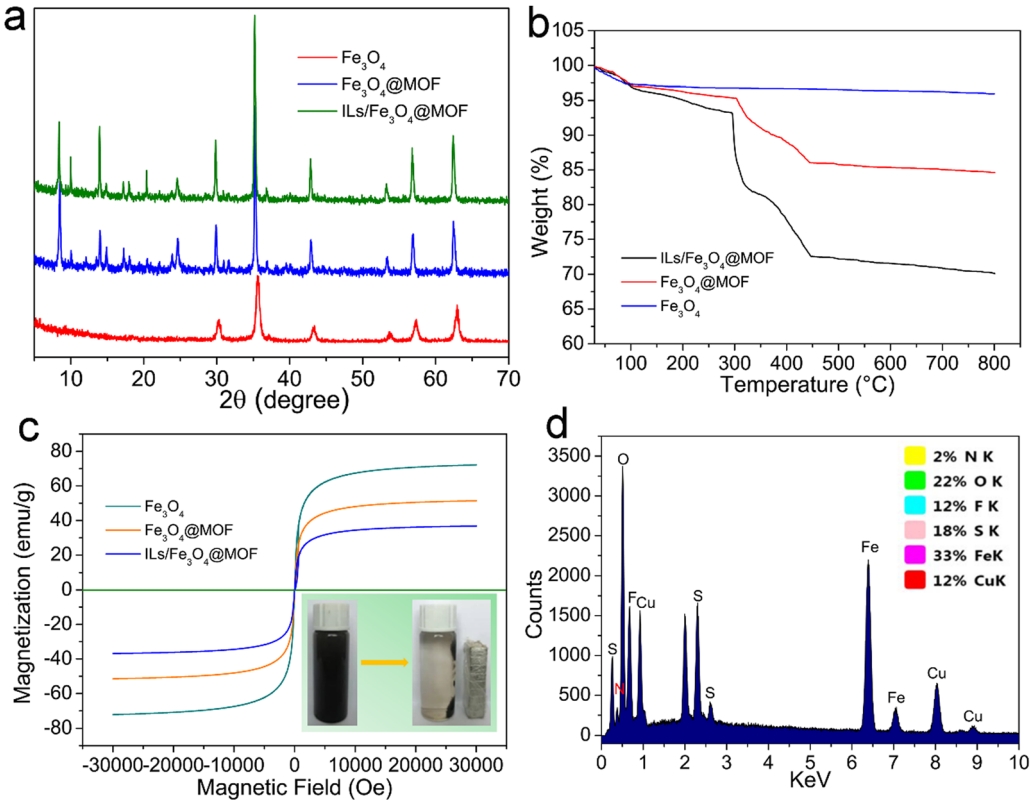


Fig. 2 (a) XRD patterns of $Fe_3O_4$ (red), $Fe_3O_4$@MOF (blue) and ILs/$Fe_3O_4$@MOF (green), (b) TG curves of $Fe_3O_4$ (blue), $Fe_3O_4$@MOF (red) and ILs/$Fe_3O_4$@MOF (blac), (c) magnetic properties of $Fe_3O_4$ (blue–green), $Fe_3O_4$@MOF (orange) and ILs/$Fe_3O_4$@MOF (blue), and (d) EDS spectrum and atomic ratio of ILs/$Fe_3O_4$@MOF.

of the composite materials were characterized and the magnetic hysteresis loops are shown in Fig. 2c. We can observe that the coercivity and remanence of all the curves are near zero, which indicates that the supports exhibit superparamagnetism.[35] This property facilitated the recovery and reusability of the immobilized lipase. The saturation magnetization (Ms) of $Fe_3O_4$@MOF and ILs/$Fe_3O_4$@MOF was 51.4 emu $g^{-1}$ and 36.7 emu $g^{-1}$, respectively, which is lower than that of $Fe_3O_4$ (72.1 emu $g^{-1}$). The MOF coating and IL introduction decreased the Ms of ILs/$Fe_3O_4$@MOF; however, the magnetic response of ILs/$Fe_3O_4$@MOF was sufficient for the magnetic separation as seen in the picture located in the lower right corner of Fig. 2c. The use of magnetic separation could reduce the loss of immobilized lipase in the reuse process.

SEM and TEM were conducted to characterize the morphologies and structural properties of $Fe_3O_4$@MOF and ILs/$Fe_3O_4$@MOF. The images (Fig. 3) revealed that $Fe_3O_4$@MOF

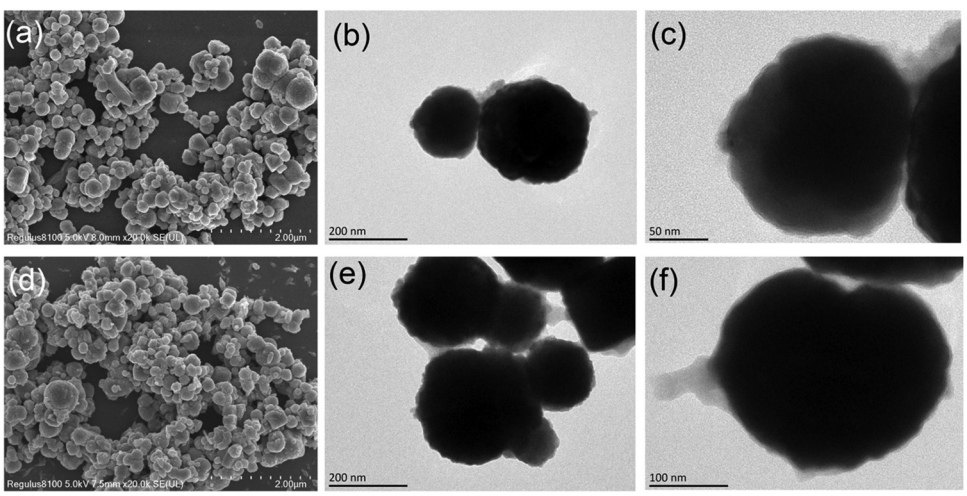


Fig. 3 SEM images of (a) $Fe_3O_4$@MOF and (d) ILs/$Fe_3O_4$@MOF. TEM images of (b and c) $Fe_3O_4$@MOF and (e and f) ILs/$Fe_3O_4$@MOF.

 

and ILs/$Fe_3O_4$@MOF were spherical nanoparticles. Nanometer size generally has a high specific surface area, which is beneficial to increasing the load of enzymes. The TEM images show that the magnetic MOF nanoparticles were core–shell structures with rough surfaces. $Fe_3O_4$ was the core of the magnetic MOF and the outside coating was composed of a Cu-based MOF. Moreover, comparing the TEM images of $Fe_3O_4$@MOF and ILs/$Fe_3O_4$@MOF, we found that the introduction of ILs did not destroy the core–shell structure. Additionally, the diameters of supports were calculated according to SEM images and the diameter distribution diagram is shown in Fig. S2 (ESI†). The statistical results showed that the average diameter of $Fe_3O_4$@MOF and ILs/$Fe_3O_4$@MOF was 257 nm and 229 nm, respectively. The addition of ILs in supports may enhance the repulsive force of particles which reduced aggregation of the particles. Therefore, we found that ILs/$Fe_3O_4$@MOF has a lower average diameter which implies better dispersibility.

In the lipase structure, a lid composed of polypeptides isolated the active center from substrates. When lipase was placed at a hydrophobic interface, interface activation occurred which opens the lid and made the active center accessible.[36] Herein, we use the water contact angle (WCA) to assess the hydrophobicity of supports and the WCA images of samples are shown in Fig. 4. The WCA of $Fe_3O_4$@MOF was 45.9°, and the WCA increased to 53.7° for ILs/$Fe_3O_4$@MOF. The increased WCA implied the hydrophobicity of ILs/$Fe_3O_4$@MOF was enhanced. When lipase is immobilized on ILs/$Fe_3O_4$@MOF, the interfacial activation may exhibit more effect on lipase which moved the lid open. The open conformation of lipase may lead to higher activity and the catalytic performance assessment supported the result.

### 3.2. Results of enzyme immobilization

Lipase was covalently immobilized on composite materials and Table 1 shows the immobilization result. From the table, we could see that lipase loadings of $Fe_3O_4$@MOF and ILs/$Fe_3O_4$@MOF were 104.7 mg $g^{-1}$ and 113.6 mg $g^{-1}$, respectively. Moreover, the prepared biocatalyst exhibited higher specific activity compared with free PPL. Specific activities of PPL-$Fe_3O_4$@MOF (534.8 U $g^{-1}$) and PPL-ILs/$Fe_3O_4$@MOF (968.4 U $g^{-1}$) increased to 1.16-fold and 2.09-fold respectively compared to free PPL. The improvement of lipase loading and activity may be due to the surface properties of MOFs. The porosity of MOFs is conducive to increasing the loading of enzymes. Moreover,

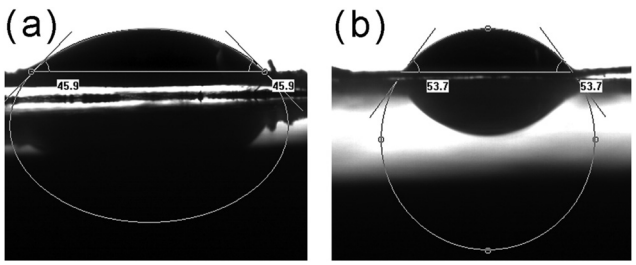


Fig. 4 Water contact angle of (a) $Fe_3O_4$@MOF and (b) ILs/$Fe_3O_4$@MOF.

Table 1 Results of lipase immobilized on magnetic MOFs[a]

| Support | Loading capacity (mg $g^{-1}$) | Immobilization yields (%) | Specific activity (U $g^{-1}$) |
|---|---|---|---|
| PPL-$Fe_3O_4$@MOF | 104.7 | 63.2 | 534.8 |
| PPL-ILs/$Fe_3O_4$@MOF | 113.6 | 71.9 | 968.4 |

[a] The activity of free PPL was 462 U $g^{-1}$ at pH = 7.0.

the MOF framework interacts with lipase molecules through covalent bonds and H bonds that led to firmly arched enzymes.[37] After ILs were introduced, the supports become more hydrophobic (as shown in Fig. 4). The lipase may exhibit an open form when immobilized on ILs/$Fe_3O_4$@MOF through interfacial activation. Meanwhile, lipase showed tendency to be adsorbed on the hydrophobic surface of ILs/$Fe_3O_4$@MOF.[38] Furthermore, the π–π stacking interaction between lipase molecules and supports was enhanced because of the introduction of the imidazole ring. The electronic interaction further enhanced the affinity of PPL and ILs/$Fe_3O_4$@MOF. The interactions between lipase and the supports on the one hand improved the microenvironment and, on the other hand, affected the structure of the immobilized enzyme. The secondary structure changes affected by immobilization were confirmed by CD spectroscopy and the detailed data are shown in Table 2.

### 3.3. Structural analysis of free and immobilized lipase

Studies have revealed that the activity and stability of lipase are related to its conformation.[39] It is known that there is a hydrophobic lid composed of an α-helical polypeptide chain that covers the active center. Through interfacial interaction between the lipase and the carrier, the conformation of the lipase can be changed, making the lid open. To investigate the mechanism of changing the catalytic performance of the immobilized lipase, the CD spectroscopy of samples were conducted and the spectra curves are shown in Fig. S3 (ESI†). The percentage of the secondary structure calculated by CDNN are listed in Table 2. It can be seen that the α-Helix percentage decreased compare with free lipase, while the β-Sheet percentage increased. The decline of α-Helix may be due to the hydrophobic interaction of the lid with the supports, which led to lid distortions and exposure of the active center. More β-Sheet is favor to the rigidity of lipase, which can improve the thermal stability and tolerance to denaturants.[40,41] The results were consistent with the findings of catalytic performance. Moreover, the results confirmed that the prepared ILs modified

Table 2 Percentage of the secondary structure of enzymes

| Biocatalyst | α-Helix (%) | β-Sheet (%) | β-Turn (%) | Random coil (%) |
|---|---|---|---|---|
| Free PPL | 25.2 | 22.7 | 19.5 | 32.2 |
| PPL-$Fe_3O_4$@MOF | 16.7 | 26.4 | 21.2 | 35.4 |
| PPL-ILs/$Fe_3O_4$@MOF | 15.3 | 28.5 | 21.5 | 34.6 |

MOFs was beneficial to the improvement of the microenvironment of enzymes.

### 3.4. Catalytic activity and stability assessment

As we know, pH and temperature play important roles in enzymatic reactions. Herein, the pH value and temperature were optimized for the hydrolysis reaction. As shown in Fig. 5a, the optimum pH for PPL-$Fe_3O_4$@MOF and PPL-ILs/$Fe_3O_4$@MOF shifted to 7.5 from 7.0, which was the optimum for free PPL. The changes may be because the $H^+$ of the solution was captured by the supports through H-bonds and ion interactions, which hindered $H^+$ from reaching enzymes. The phenomenon of optimum pH shifts was consistent with the previous report.[42] The shift of optimum pH enhanced the tolerance of immobilized lipase to a higher pH value. When the pH rose to 8.5, PPL-ILs/$Fe_3O_4$@MOF maintained 90.2% of its initial activity, while free PPL and PPL-$Fe_3O_4$@MOF retained 65.4% and 84.5% of their initial activity, respectively.

We could see that from Fig. 5b, the optimum reaction temperature for PPL-ILs/$Fe_3O_4$@MOF and PPL-$Fe_3O_4$@MOF was 45 °C, while that for free PPL was 40 °C. When the temperature rose to 60 °C, residual activities for free PPL rapidly reduced to 52.6%, while the value for PPL-ILs/$Fe_3O_4$@MOF and PPL-$Fe_3O_4$@MOF was 82.3% and 73.1%, respectively. The results indicate that lipase was more stable at a higher temperature after being immobilized. This may be because the interaction between lipase and supports firmly anchored the structure of enzymes, which protected the integrity of lipase.

The stability of immobilized lipase plays an important role in its application. In this work, urea was used to test the tolerance of immobilized lipase to denaturant. As shown in Fig. 5c, the relative activity decreased when the urea concentration increased. When urea concentration rose to 6 M, residual activity for PPL-$Fe_3O_4$@MOF, PPL-ILs/$Fe_3O_4$@MOF and free PPL was 49.6%, 66.2% and 10.2%, respectively. The results indicate that lipase resistance to denaturants was enhanced after immobilized on the prepared supports. In addition, compared with PPL-$Fe_3O_4$@MOF, PPL-ILs/$Fe_3O_4$@MOF further enhanced the tolerance of lipase to denaturant. The improvement may be due to the interaction between the carrier and urea molecules, which prevented urea from disrupting the structure of lipase.[43] On the other hand, the multiple interactions between the enzyme and carrier strengthened the rigidity and integrity of lipase, which was further analyzed in the secondary structure investigation.

Good reusability can save costs for the application of enzymes, while convenient separation performance can increase production efficiency. PPL-$Fe_3O_4$@MOF and PPL-$Fe_3O_4$@MOF have strong magnetic responsiveness which improved the biocatalyst recovery. The magnetic separation may reduce the loss of biocatalyst and guarantee that the activity was not affected by the separation process. As seen in Fig. 5d, PPL-ILs/$Fe_3O_4$@MOF and PPL-$Fe_3O_4$@MOF maintained 70.2% and 63.4% of the initial activity after eight cycles, respectively. The results indicated that the magnetic MOF nanoparticles have good mechanical strength and that the carrier provided an excellent microenvironment for the

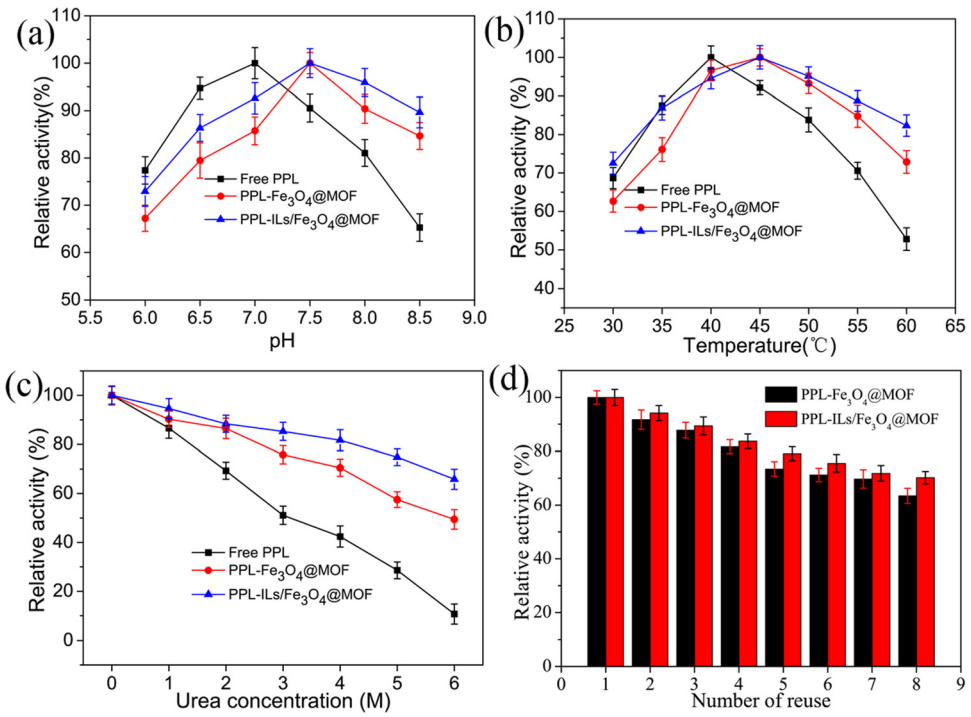


Fig. 5 Catalytic performance of lipase under different conditions. Effect of (a) pH, (b) temperature, and (c) denaturant concentration on lipase activity. (d) Reusability of immobilized lipase in the hydrolysis reaction.

 

immobilized lipase. The introduction of ILs can prevent organic solvent molecules and ions in solution from denaturing the lipase through π–π stacking, H-bonding, ion interaction, and coordination bonding.[44] The porosity of MOFs is conducive to improving transfer rates of substrates and products, which reduced the inactivation rate of the enzyme.

### 3.5. Application of immobilized lipase in the synthesis of a flavor ester

Compared with the chemical synthesis of isoamyl acetate, biocatalysis is more eco-friendly. Here, we used the prepared immobilized lipase to catalyze the synthesis of isoamyl acetate through esterification in an organic solvent. The optimized reaction conditions are shown in Fig. 6.

As shown in Fig. 6a, the ester yield increased as the molar ratio of alcohol/acid rose to 3 : 1 from 1 : 1. This may be because the esterification reaction is reversible and because an appropriate amount of alcohol can promote the formation of esters while excess alcohol can strengthen the mutual collision between substrates.[45] However, when the molar ratio of alcohol/acid increases from 3 : 1 to 5 : 1, the ester yield decreased because of the high concentration of isoamyl alcohol, which would cause an irreversible denaturation of the enzyme molecules.

We can observe from Fig. 6b that the ester yield increased when reaction temperature ranged in 35–45 °C. This phenomenon may be because, for an endothermic reaction, the increase in temperature can enhance the thermal movement of substrate molecules and promote the synthesis of products. When reaction temperature increased in the range of 45–55 °C, the ester yield decreased. This is because an extremely high temperature will cause lipase denaturation and inactivation, resulting in a decrease in substrate conversion. The ester yield of PPL-ILs/$Fe_3O_4$@MOF was 59.6% higher than that of PPL-$Fe_3O_4$@MOF (52.7%) at 45 °C. The result demonstrated that the ILs was beneficial to lipase activity because of the H-bonding, π–π stacking, and electronic interaction between ILs and lipase.

Enzymatic esterification usually occurs in organic solvents, which promotes the reaction equilibrium in ester synthesis because of the mutual solubility of solvent and esters. The polarity and hydrophobicity of solvents could intensely affect the catalytic performance of lipase. As observed in Fig. 6c, the reaction showed the highest ester yield in hexane. This may be because hexane has an appropriate hydrophobicity that does not affect the enzyme's micro water layer.[6]

Lipase catalytic esterification is a time-consuming, multi-step, and complex reaction, and the reaction time effect on the ester yield is shown in Fig. 6d. Under optimized substrate molar ratio, temperature and solvent, the ester yield increased rapidly within the first 12 h and the yield for PPL-ILs/$Fe_3O_4$@-MOF and PPL-$Fe_3O_4$@MOF reached 65.3% and 58.9%, respectively. When the reaction lasted for 24 h, the ester yield for PPL-ILs/$Fe_3O_4$@MOF and PPL-$Fe_3O_4$@MOF increased to 75.2% and 71.3%, respectively. Lipase should be surrounded by a water layer that maintains the catalytic activity of the enzyme. In the first 12 h, the reaction provided sufficient water for lipase activity to enable the ester yield to increase rapidly. The esterification and hydrolysis reactions gradually reached equilibrium over time, such that the ester yield no longer increases.

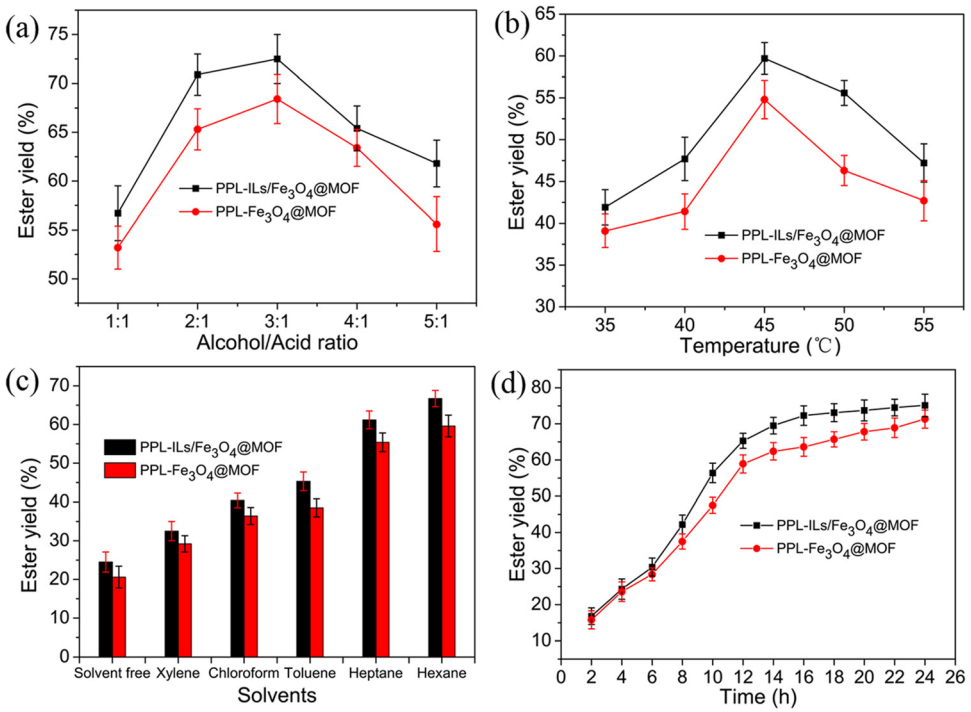


Fig. 6 Optimization of (a) alcohol/acid molar ratio, (b) reaction temperature, (c) reaction solvents and (d) reaction time for the synthesis of isoamyl acetate.

Considering the relationship between the reaction time and ester yield, we think that the optimum reaction time was 16 h, while the ester yield was 72.3%.

## 4. Conclusions

In summary, imidazolium-based ILs with $[NTf_2]^-$ as the anion-modified magnetic Cu-based MOF nanocomposites were successfully prepared and used as supports for PPL immobilization through covalent bond. Lipase molecules interacted with MOFs and ILs through multiple interactions which caused conformation changes approved by CD spectroscopy. The prepared supports provided a good microenvironment for lipase, which enhanced catalytic performance in the hydrolysis of esters and synthesis of isoamyl acetate. The ester yield can reach up to 75.2% under optimized reaction conditions. In addition, on one hand, the activity and stability were enhanced after immobilization; on the other hand, the application of magnetic separation decreased the inactivation and leakage of enzymes compared with centrifugation and filtration separation. This research work is helpful in the promotion of the further application of MOF and IL composites in the field of enzyme immobilization.

## Author contributions

Hongbo Suo: conceptualization, data curation, investigation, methodology, writing – original draft. Huining Geng: data curation, formal analysis, investigation, validation, writing – original draft. Lu Zhang: methodology, software, validation, visualization. Guoyun liu: data curation, methodology, project administration, resources. Hui Yan: resources, validation, visualization,writing – review & editing. Rui Cao: data curation, investigation, methodology. Jiahao Zhu: methodology, validation, visualization. Yi Hu: conceptualization, project administration, resources, supervision, writing – review & editing. Lili Xu: conceptualization, funding acquisition, methodology, supervision, writing – review & editing.

## Conflicts of interest

The authors declare there are no competing financial interest.

## Acknowledgements

This work was financially supported by the National Natural Science Foundation of China (No. 81901420), the Natural Science Foundation of Shandong Province (ZR2022MB125) and the Research Fund of Liaocheng University (No. 318012106, 318052027, and 318052028).

## References

1 M. Zare, M.-T. Golmakani and M. Niakousari, *LWT*, 2019, **101**, 214–219.
2 N. Yusoff Azudin, S. Sangaran and S. R. Abd Shukor, *J. Environ. Chem. Eng.*, 2020, **8**, 103186.
3 Y. Liu, X. WeiZhuo and X. Wei, *Food Chem. Adv.*, 2022, **1**, 100052.
4 K. Vivek, G. S. Sandhia and S. Subramaniyan, *Biotechnol. Adv.*, 2022, **60**, 108002.
5 S. Asmat, A. H. Anwer and Q. Husain, *Int. J. Biol. Macromol.*, 2019, **140**, 484–495.
6 H. Aghaei, A. Yasinian and A. Taghizadeh, *Int. J. Biol. Macromol.*, 2021, **178**, 569–579.
7 C. Vasilescu, A. Todea, A. Nan, M. Circu, R. Turcu, I.-C. Benea and F. Peter, *Food Chem.*, 2019, **296**, 1–8.
8 G. Chen, I. M. Khan, W. He, Y. Li, P. Jin, O. H. Campanella, H. Zhang, Y. Huo, Y. Chen, H. Yang and M. Miao, *Compr. Rev. Food Sci. Food Saf.*, 2022, **21**, 2688–2714.
9 G. Hu, Z. Li, D. Ma, C. Ye, L. Zhang, C. Gao, L. Liu and X. Chen, *Nat. Catal.*, 2021, **4**, 395–406.
10 Q. Ding, D. Ma, G.-Q. Liu, Y. Li, L. Guo, C. Gao, G. Hu, C. Ye, J. Liu, L. Liu and X. Chen, *Nat. Commun.*, 2020, **11**, 2262.
11 W. Shuai, R. K. Das, M. Naghdi, S. K. Brar and M. Verma, *Biotechnol. Appl. Biochem.*, 2017, **64**, 496–508.
12 T. Matsumoto, R. Yamada and H. Ogino, *World J. Microbiol. Biotechnol.*, 2019, **35**, 193.
13 W. Xie and M. Huang, *Energy Convers. Manage.*, 2018, **159**, 42–53.
14 R. C. Rodrigues, J. J. Virgen-Ortíz, J. C. S. dos Santos, Á. Berenguer-Murcia, A. R. Alcantara, O. Barbosa, C. Ortiz and R. Fernandez-Lafuente, *Biotechnol. Adv.*, 2019, **37**, 746–770.
15 J. Cui, S. Ren, B. Sun and S. Jia, *Coord. Chem. Rev.*, 2018, **370**, 22–41.
16 S. Liang, X.-L. Wu, J. Xiong, M.-H. Zong and W.-Y. Lou, *Coord. Chem. Rev.*, 2020, **406**, 213149.
17 W. Duan, Z. Zhao, H. An, Z. Zhang, P. Cheng, Y. Chen and H. Huang, *Top. Curr. Chem.*, 2019, **377**, 34.
18 J. Mehta, N. Bhardwaj, S. K. Bhardwaj, K.-H. Kim and A. Deep, *Coord. Chem. Rev.*, 2016, **322**, 30–40.
19 W. Xie and X. Zang, *Food Chem.*, 2017, **227**, 397–403.
20 W. Xie and X. Zang, *Food Chem.*, 2016, **194**, 1283–1292.
21 S. S. Nadar and V. K. Rathod, *Int. J. Biol. Macromol.*, 2018, **120**, 2293–2302.
22 C. Zhang and X. Cai, *Compos. Interfaces*, 2019, **26**, 379–396.
23 Y. Li, T. Jing, G. Xu, J. Tian, M. Dong, Q. Shao, B. Wang, Z. Wang, Y. Zheng, C. Yang and Z. Guo, *Polymer*, 2018, **149**, 13–22.
24 I. A. Trindade Ximenes, P. C. O. de Oliveira, C. A. Wegermann and M. C. de Moraes, *J. Pharm. Biomed. Sci.*, 2021, **204**, 114286.
25 J. C. S. d Santos, O. Barbosa, C. Ortiz, A. Berenguer-Murcia, R. C. Rodrigues and R. Fernandez-Lafuente, *ChemCatChem*, 2015, **7**, 2413–2432.
26 K. C. Badgujar, V. C. Badgujar and B. M. Bhanage, *Curr. Opin. Green Sustainable Chem.*, 2022, **36**, 100621.
27 A. Schindl, M. L. Hagen, S. Muzammal, H. A. D. Gunasekera and A. K. Croft, *Front. Chem.*, 2019, **7**, 347.
28 X. Xiang, S. Ding, H. Suo, C. Xu, Z. Gao and Y. Hu, *Carbohydr. Polym.*, 2018, **182**, 245–253.

 

29 W. Xie and X. Zang, *Food Chem.*, 2018, **257**, 15–22.
30 H. Suo, M. Li, R. Liu and L. Xu, *Colloids Surf., B*, 2021, **206**, 111960.
31 L. Wang, W. Zhi, J. Wan, J. Han, C. Li and Y. Wang, *ACS Sustainable Chem. Eng.*, 2019, **7**, 3339–3348.
32 Y. Yuan, W. Cai, J. Xu, J. Cheng and K.-S. Du, *Colloids Surf., B*, 2021, **204**, 111792.
33 C. Wang, H. Luo, X. Luo, H. Li and S. Dai, *Green Chem.*, 2010, **12**, 2019–2023.
34 F. Ghourchian, N. Motakef-Kazemi, E. Ghasemi and H. Ziyadi, *J. Environ. Chem. Eng.*, 2021, **9**, 106388.
35 R. Zhai, Y. Yuan, F. Jiao, F. Hao, X. Fang, Y. Zhang and X. Qian, *Anal. Chim. Acta*, 2017, **994**, 19–28.
36 J. Zhang, Z. Wang, W. Zhuang, H. Rabiee, C. Zhu, J. Deng, L. Ge and H. Ying, *ACS Appl. Mater. Interfaces*, 2022, **14**, 39622–39636.
37 M. C. Bourkaib, P. Gaudin, F. Vibert, Y. Guiavarc'h, S. Delaunay, X. Framboisier, C. Humeau, I. Chevalot and J.-L. Blin, *Microporous Mesoporous Mater.*, 2021, **323**, 111226.
38 M. Mathesh, B. Luan, T. O. Akanbi, J. K. Weber, J. Liu, C. J. Barrow, R. Zhou and W. Yang, *ACS Catal.*, 2016, **6**, 4760–4768.
39 S. Sáringer, T. Valtner, Á. Varga, J. Maléth and I. Szilágyi, *J. Mater. Chem. B*, 2022, **10**, 2523–2533.
40 S. Asmat, Q. Husain, M. Shoeb and M. Mobin, *Mater. Sci. Eng., C*, 2020, **112**, 110883.
41 S. Wei, X. Zou, J. Tian, H. Huang, W. Guo and Z. Chen, *J. Am. Chem. Soc.*, 2019, **141**, 20335–20343.
42 M. Sarno, M. Iuliano, M. Polichetti and P. Ciambelli, *Process Biochem.*, 2017, **56**, 98–108.
43 L. Xu, R. Liu, Z. Li, M. Li, M. Zhao, Y. Li, G. Hou, A. Li and H. Suo, *Ind. Eng. Chem. Res.*, 2022, **61**, 1277–1284.
44 J. Cui, T. Kobayashi, R. L. Sacci, R. A. Matsumoto, P. T. Cummings and M. Pruski, *J. Phys. Chem. B*, 2020, **124**, 9931–9937.
45 S. Ji, W. Liu, S. Su, C. Gan and C. Jia, *LWT*, 2021, **149**, 111897.